Nanoscale

Interplay Between Microstructure, Defect States, and Mobile Charge Generation in Transition Metal Dichalcogenide Heterojunctions

Journal:	*Nanoscale*
Manuscript ID	NR-ART-01-2021-000384.R1
Article Type:	Paper
Date Submitted by the Author:	05-Apr-2021
Complete List of Authors:	Sulas-Kern, Dana; National Renewable Energy Laboratory, Zhang, Hanyu; national renewable energy laboratory, Nanoscience and Chemistry Li, Zhaodong; National Renewable Energy Laboratory Blackburn, Jeffrey; NREL,

Interplay Between Microstructure, Defect States, and Mobile Charge Generation in Transition Metal Dichalcogenide Heterojunctions

Dana B. Sulas-Kern, Hanyu Zhang, Zhaodong Li, Jeffrey L. Blackburn**

National Renewable Energy Laboratory, 15013 Denver West Parkway, Golden, CO 80401

Abstract – Two-dimensional transition metal dichalcogenides (2D-TMDCs) have gained attention for their promise in next-generation energy-harvesting and quantum computing technologies, but realizing these technologies require a greater understanding of TMDC properties that influence their photophysics. To this end, we discuss here the interplay between TMDC microstructure and defects with the charge generation yield, lifetime, and mobility. As a model system, we compare monolayer-only and monolayer-rich MoS_2 grown by chemical vapor deposition, and we employ the TMDCs in Type-II charge-separating heterojunctions with semiconducting single-walled carbon nanotubes (s-SWCNTs). Our results suggest longer lifetimes and higher yields of mobile carriers in samples containing a small fraction of defect-rich multilayer islands on predominately monolayer MoS_2. Compared to the monolayer-only heterojunctions, the carrier lifetimes increase from 0.73 μs to 4.71 μs, the hole transfer yield increases from 23% to 34%, and the electron transfer yield increases from 39% to 59%. We reach these conclusions using a unique combination of microwave photoconductivity (which probes only mobile carriers) along with transient absorption spectroscopy (which identifies spectral signatures unique to each material and type of photoexcited quasiparticle, but does not probe mobility). Our results highlight the substantial changes in photophysics that can occur from small changes in TMDC microstructure and defect density, where the presence of defects does not necessarily preclude improvements in charge generation.

Introduction

Two-dimensional transition metal dichalcogenides (2D-TMDCs) offer promising optoelectronic and quantum properties for the development of next-generation semiconductor technologies including applications in energy harvesting, quantum computing, and photocatalysis.[1] Importantly, the success of these TMDC-based technologies relies on increasing the lifetimes and mobilities of photogenerated charge carriers. For example, while exciton-dominated decay kinetics result in ultrafast relaxation in MoS_2 monolayers over femtoseconds to nanoseconds,[2-4] generation of longer-lived free charge carriers is needed to enable carrier motion to photocatalytic sites for redox reactions, charge extraction at electrodes in photovoltaics or photodetectors, and binary information transmission in computing systems through sustained electronic spin and momentum degrees of freedom.

Despite the obvious need to extend carrier lifetimes, the path toward sustaining sufficiently long-lived carriers in high yields is not yet well defined. TMDC recombination dynamics vary widely depending on factors such as thickness,[5-8] grain size,[8-9] edge states,[10] vacancy or defect concentration,[11-13] doping,[14-15] substrate,[7, 16] ambient conditions,[17] and fabrication method.[10] Longer-lived kinetics are generally expected in multilayers compared to monolayers due to both a transition to an indirect bandgap as well as the decreasing impact of surface recombination.[5] While some studies do observe predictable trends such as increasing lifetime with the number of layers,[5] in other cases multilayer materials exhibit even shorter effective lifetimes compared to the monolayer counterparts.[7] The complex interplay of factors that affect excited state dynamics, and sometimes mask expected trends, highlights the need for a greater fundamental understanding of structure-property relationships in this emerging class of materials.

TMDC defects are key factors that complicate carrier kinetics,[11-13] leading to important impacts on device-relevant properties such as electronic transport[18-19] and photocatalytic activity.[20-21] On one hand, defects

can rapidly quench TMDC excited states,[22] and localized disorder around point defects such as molybdenum antisites has been shown to create charge scattering centers that decrease band-like mobility.[23] On the other hand, defects such as sulfur vacancies in MoS_2 have been shown to enable hopping-type charge transport to decrease intra-grain sheet resistance,[19] and defects such as edge states, vacancies, and strained regions have been increasingly recognized as a means to enhance redox reaction rates and yields while decreasing the necessary overpotential.[20-21] These various roles of defects in TMDC performance highlight the fact that it is currently unclear whether defects should be minimized or utilized to advance different types of optoelectronic or photocatalytic applications.

In addition to understanding and optimizing intrinsic TMDC properties, a fruitful strategy to increase the lifetimes and yields of free charge carriers is to employ TMDCs in heterojunctions with materials having appropriate energy-level offsets to overcome the binding energies of photogenerated excitons.[1, 24-27] While this has been successful for generating free carriers persisting into the tens of nanosecond and microsecond timescales,[24, 28] it is important to note that the photophysical processes at the heterojunction are substantially affected by the underlying TMDC properties such as defects,[29] thicknesses,[25, 27] and interface states.[25] Perhaps due to the developing state of TMDC syntheses and variations in the resulting materials, it is not uncommon for studies to report differing photophysics and extents of charge transfer even for nominally similar heterojunctions.[30-31]

Here, we discuss the interplay between TMDC defect states and microstructure along with the ability to generate long-lived mobile charge carriers when employed in heterojunctions. As a model system, we compare monolayer-only and monolayer-rich MoS_2 grown by chemical vapor deposition (CVD), and we employ the TMDCs in Type-II charge-separating heterojunctions with semiconducting single-walled carbon nanotubes (s-SWCNTs). Interestingly, our results suggest that the presence of defect-rich multilayer islands on predominately monolayer MoS_2 (1) increases free carrier mobility, (2) generates persistent photoconductivity in the MoS_2 layer, (3) extends carrier lifetimes by approximately a factor of 6 in the SWCNT layer (from 0.73 μs to 4.71 μs), and (4) enhances the charge generation yield by ~50%. We reach these conclusions using a unique combination of time-resolved and quasi-steady-state microwave photoconductivity to probe only the mobile population of free carriers along with quantitative analysis of transient absorption data that provide spectral signatures to differentiate between excitons, charges, and defects. Our results highlight an interesting balance between microstructure and defect density, where carrier generation appears to be improved by a small fraction of multilayer sites despite the presence of more defects in this system.

Results

Monolayer-Only vs. Monolayer-Rich MoS_2

We investigate the microstructure-dependent excited state kinetics in CVD-grown MoS_2 that is either monolayer-only (Figure 1a) or monolayer-rich (Figure 1b). The photoluminescence (PL) image for the monolayer-only sample in Figure 1a maps the characteristic monolayer A-exciton PL centered at 660 nm, which appears to be largely uniform.[24] However, the 660 nm PL image in Figure 1b has several ~1 μm diameter dark islands which have <20% PL intensity relative to the maximum PL signal in Figure 1b. These islands appear within ripples having ~80% PL intensity relative to the maximum value.

Using Raman spectroscopy (Figure 1c) and atomic force microscopy (AFM, see Section S2), we identify the dark PL regions in Figure 1b as multilayer sites. We find that ~0.8% area of the predominately monolayer sample contains islands that are on average 360 +/- 100 nm wide and 90 +/- 40 nm tall (~130 layers). We therefore refer to this microstructure as 0.8%-multilayer MoS_2. This large thickness indicates that the multilayer regions likely have characteristics of

bulk MoS_2. The PL at multilayer sites appears dark because the indirect band gap decreases the PL quantum yield and shifts the PL peak to longer wavelengths (i.e. ~950 nm for bulk *versus* ~660 nm for monolayer).[32] The dark regions in the PL map appear larger than the actual diameter of the multilayer regions primarily due to the spatial resolution of the of the optical system. Exciton quenching due to band offsets at the monolayer/multilayer (1L/nL) interfaces may also contribute to a larger region of PL quenching around the multilayer sites.[33-36]

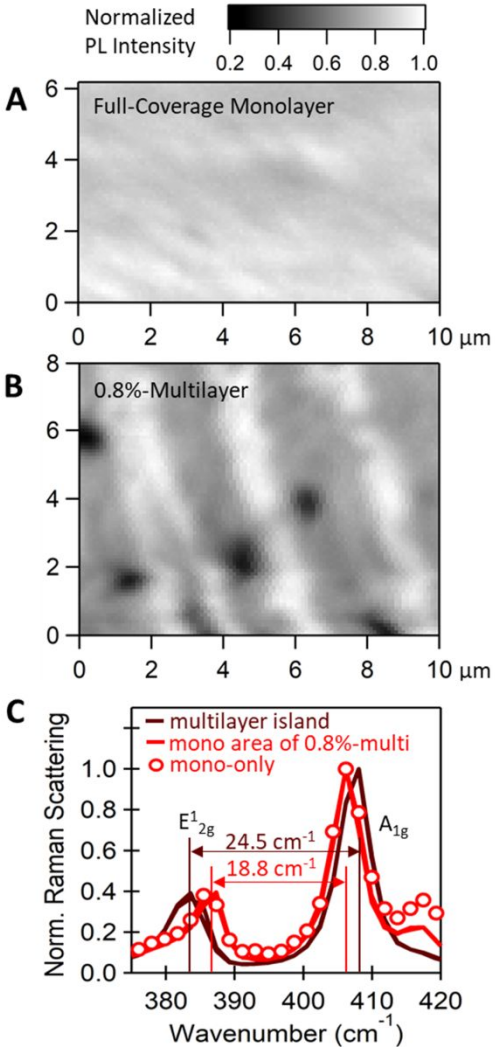

Figure 1. *Photoluminescence (PL) maps at 660 nm corresponding to monolayer MoS_2 A-exciton PL peak measured using 532 nm excitation for (a) full-coverage monolayer MoS_2 and (b) predominately monolayer MoS_2 containing 0.8% area multilayer islands; (c) Raman scattering at the MoS_2 E^1_{2g} and A_{1g} modes showing larger peak difference at the multilayer islands.*

Figure 1c shows the in-plane (E^1_{2g}) and out-of-plane (A_{1g}) Raman scattering modes for the monolayer-only sample along with the 0.8%-multilayer sample at monolayer or multilayer regions. The majority of both samples are continuous monolayers with 18.8 cm^{-1} energy difference between the E^1_{2g} and A_{1g} peaks.[37] The multilayer islands exhibit a larger peak difference of 24.5 cm^{-1}, characteristic of bulk MoS_2.[37]

We note that the ~20% variation of PL intensity within the monolayer-only MoS_2 areas is not unusual for CVD-grown materials. Ripple effects have been attributed to variations in strain, doping, wrinkles, and grain boundaries.[38-40] We also observe up to 10 nm redshift of the PL spectrum in the regions with ~80% PL intensity relative to the maximum sample PL intensity, similar to the variations in PL peak wavelength for monolayer samples reported by others.[40] Interestingly, the multilayer islands appear to grow primarily within the monolayer areas that have red-shifted, lower-intensity PL. While the reason for this correlation requires further study, it may indicate that inhomogeneously distributed strain or doping either causes the growth of multilayer sites, or (perhaps more likely) these effects result from multilayer islands that are seeded before the growth of the monolayer.

Effect of TMDC Thickness Inhomogeneity in MoS_2 / SWCNT Heterojunctions

Our previous study showed that the Type-II band offset at monolayer MoS_2/(6,5)-SWCNT interfaces separates tightly bound excitons, generating long-lived charge carriers that persist up to microsecond timescales at room temperature.[24] However, the addition of multilayer islands to predominately monolayer TMDCs results in several new photophysical pathways, as illustrated in Figure 2.

Figure 2 illustrates energy level offsets in MoS_2/SWCNT heterojunctions containing regions of both monolayer (1L) and multilayer

(nL) MoS_2. We estimate the energetics of the nL regions assuming the bulk limits for MoS_2. The diagram does not include defect states or band bending at the interfaces, though both defects and band bending are expected to have important impacts on charge transfer at TMDC homojunction[41] and heterojunction[27] interfaces.

The MoS_2/SWCNT interfaces form Type-II heterojunctions at both the 1L and nL MoS_2 areas. Varying MoS_2 thickness affects the MoS_2 valence band maximum (*i.e.* ionization potential, IP) much more strongly than the conduction band minimum (*i.e.* electron affinity, EA).[42] For this reason, increasing MoS_2 thickness significantly decreases the driving force for hole transfer from MoS_2 to the SWCNTs, while increasing MoS_2 thickness slightly increases the driving force for electron transfer from the SWCNTs to MoS_2.

We estimate the thermodynamic driving force for charge generation using the free energy change (ΔG) upon electron transfer (ET) or hole transfer (HT) as $\Delta G_{ET/HT} = (IP_D - EA_A) - E_{opt,D/opt,A}$, where D and A refer to the donor and acceptor, and E_{opt} is the optical gap. We summarize ΔG_{CT} values at various interfaces in Table 1.

Table 1. *Estimated change in free energy (ΔG) for electron transfer (ET) or hole transfer (HT) at various interfaces estimated from literature values of electron affinity and ionization potential*[27, 43-47]

ΔG_{HT} 1L-MoS_2 to SWCNT	-620 +/- 90 meV
ΔG_{HT} nL-MoS_2 to SWCNT	-70 +/- 90 meV
ΔG_{ET} SWCNT to 1L-MoS_2	0 +/- 90 meV
ΔG_{ET} SWCNT to nL-MoS_2	-20 +/- 90 meV

We note that it is uncertain whether 1L/nL MoS_2 interfaces form Type-I or Type-II homojunctions because of the variation in reported MoS_2 band energies,[27, 43-46] differing sensitivity of monolayer and multilayer energies to substrate effects and atmospheric adsorbates,[35] and possible band bending.[41] While calculations of the layer-dependence for pure band energetics would suggest Type-I band alignment at 1L/nL interfaces,[34] others have observed Type-II rectifying diodes at 1L/nL junctions likely caused by interface characteristics that can alter the small relative offset of EA energies.[35] If the system is Type-II, we estimate the driving force for hole transfer from 1L to nL MoS_2 around -450 +/- 130 meV, but due to the small EA offset, exciton energy transfer can also compete with hole transfer. The energetics in Figure 2 suggest that exciton separation *via* electron transfer at 1L/nL interfaces should be unfavorable with positive ΔG_{ET}. However, the small difference in electron

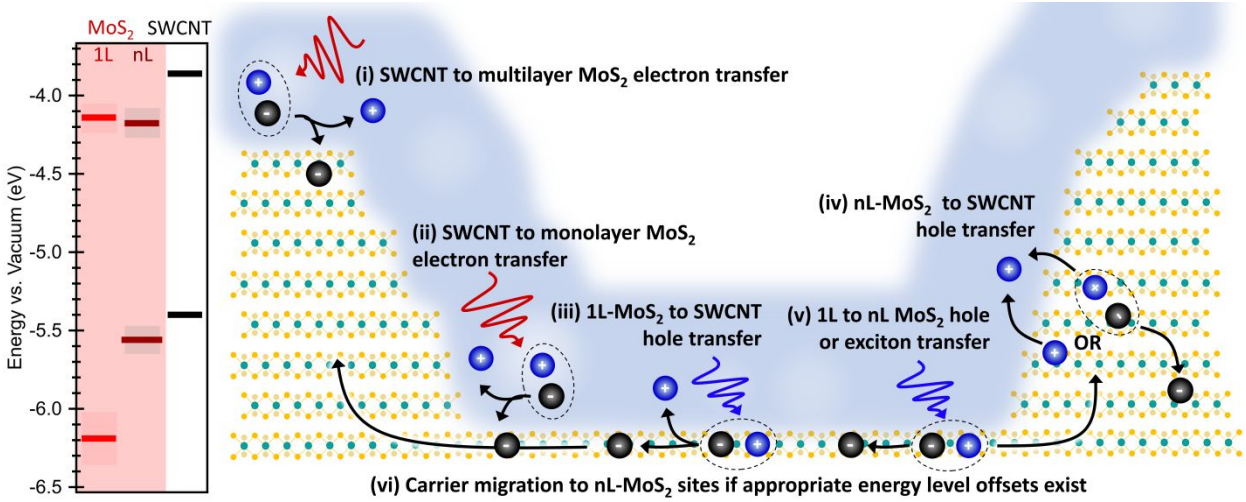

Figure 2. *Energy level diagram for monolayer(1L)/multilayer(nL)-MoS_2/SWCNT heterojunctions with energy levels from References 27, 43-47. Schematic illustrates several charge transfer and energy transfer processes likely to occur upon photoexcitation.*

affinity could possibly facilitate migration of free electrons to multilayer sites.

The illustration in Figure 2 summarizes the most likely photophysical processes. Briefly, excitons generated on the SWCNT layer can undergo electron transfer at nL (process i) or 1L (process ii) MoS_2 sites. MoS_2 photoexcitation leads to hole transfer to SWCNTs with a larger driving force at 1L-MoS_2 areas compared to nL-MoS_2 areas (processes iii and iv). Additional charge separation may occur at 1L/nL interfaces *via* hole transfer to multilayer sites, where this process competes with exciton energy transfer (process v). This 1L/nL interaction provides an additional pathway for hole transfer from nL-MoS_2 to the SWCNT layer *via* transfer of free holes separated at the 1L/nL interface (process iv). This diagram serves to give a general overview of simplest possible case for photophysical processes in 1L/nL-MoS_2/SWCNT heterojunctions, though in the following discussion we show that other factors such as defect states can further affect the observed photophysics.

Small Fraction of MoS_2 Multilayers Increases Carrier Lifetimes and Charge Transfer Yields

Since efficient charge generation is essential for optimized performance in TMDC-based applications, we use transient absorption (TA) spectroscopy to compare carrier lifetimes and yields between MoS_2/SWCNT heterojunctions made using the monolayer-only or monolayer-rich MoS_2.

Figure 3a shows the microsecond time-range carrier lifetimes for the 0.8%-multilayer-MoS_2/SWCNT and 1L-MoS_2/SWCNT heterojunctions measured with TA. We characterize the carrier lifetimes based on the SWCNT trion induced absorption signature (X^+, Figure 3b), as discussed in Reference 24 and Section S3. The 0.8%-multilayer MoS_2/SWCNT heterojunction exhibits significantly longer-lived kinetics compared to the monolayer-only heterojunction, where the amplitude-average lifetime increases from $\tau_{mono\text{-}only\text{-}HJ}$ = 0.73 µs to $\tau_{0.8\%\text{-}multi\text{-}HJ}$ = 4.71 µs (see Table S1 for multiexponential fitting components).

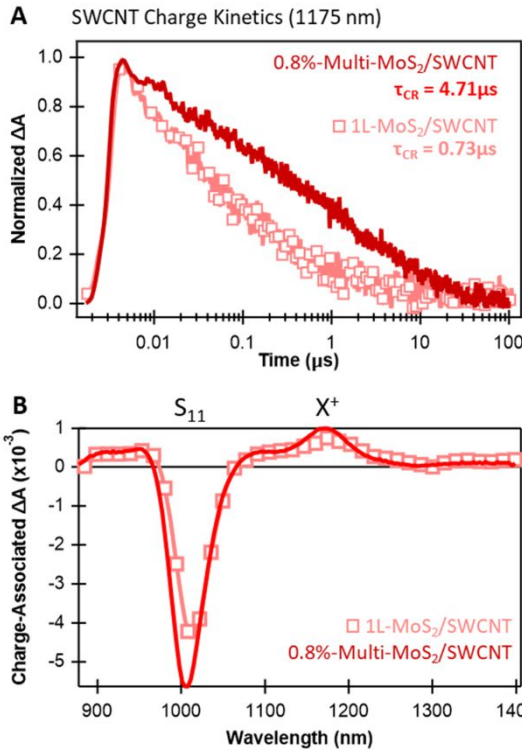

Figure 3. *(a) Kinetic traces at the SWCNT trion induced absorption (1175 nm) following 440nm excitation at 1.2 x 10^{12} absorbed photons cm^{-2}, showing charge-recombination time (τ_{CR}) of 4.71 µs in the 0.8%-multilayer-MoS_2/SWCNT heterojunction (dark red trace) compared to τ_{CR} of 0.73 µs the monolayer-only MoS_2/SWCNT heterojunction (light red squares). (b) Fitted charge-associated spectrum at the time of maximum charge separation (~3 ps) showing greater intensity in 0.8%-multi-MoS_2/SWCNT for the SWCNT S_{11} ground state bleach and trion (X+) induced absorption.*

The charge-transfer yield (φ_{CT}) is also higher in 0.8%-multilayer MoS_2/SWCNT. Figure 3b shows the charge-associated TA component that we obtain from global target analysis at the time when charge separation is maximized in these heterojunctions (~3 ps) following MoS_2 selective excitation at 440 nm. The charge-associated spectra have the same shape for both heterojunctions, but the spectrum has higher S_{11} ground state bleach and trion (X^+) intensity in the

0.8%-multilayer MoS_2/SWCNT heterojunction. We estimate φ_{CT} based on these SWCNT trion induced absorption intensities, as further described in Reference 24 and Section S3. Table 2 shows the corresponding φ_{CT} for both SWCNT to MoS_2 electron transfer and MoS_2 to SWCNT hole transfer. We find that both the φ_{ET} and φ_{HT} increase by ~50% in the samples with multilayer MoS_2 islands compared to the monolayer-only heterojunction.

Table 2. Estimated electron-transfer yield (φ_{ET}) following selective SWCNT excitation at 1000 nm and hole transfer yield (φ_{HT}) following selective MoS_2 excitation at 440 nm along with the amplitude-averaged charge recombination lifetime (τ_{CR})

	φ_{ET}	φ_{HT}	τ_{CR} (μs)
Mono-only MoS_2/SWCNT	23%	39%	0.73
0.8%-Multi MoS_2/SWCNT	34%	59%	4.71

MoS_2 with Multilayer Islands Enhances Photoconductivity in SWCNT Heterojunctions

Although TA spectroscopy is often used to identify spectral signatures that are associated with charge generation, such as the SWCNT trion induced absorption in Figure 3, TA spectroscopy does not measure whether those carriers are mobile. For this reason, we pair our TA studies with microwave photoconductivity, which probes only the mobile carrier population.[48]

Microwave photoconductivity has long been used for contactless characterization of minority carrier lifetimes and mobility in photoactive semiconductors, and related methods have even been considered commercially as a relatively straight forward way to assess semiconductor quality and impurity distributions in silicon bricks before they are cut into wafers for solar cells.[49-52] Here, we perform both quasi-steady-state and time-resolved microwave photoconductivity (SSMC and TRMC, respectively). Both methods rely on an impedance-matched circuit containing the sample of interested within a microwave waveguide. Light incident on the sample through the waveguide increases the sample conductivity through photo-induced charge generation, disrupting the impedance matching and causing a change in the microwave reflectivity. In SSMC, we vary the wavelength of incident light to obtain a spectral profile of the sample conductivity. In TRMC, we measure the transient decay of the photoconductance following a 5 ns laser pulse.

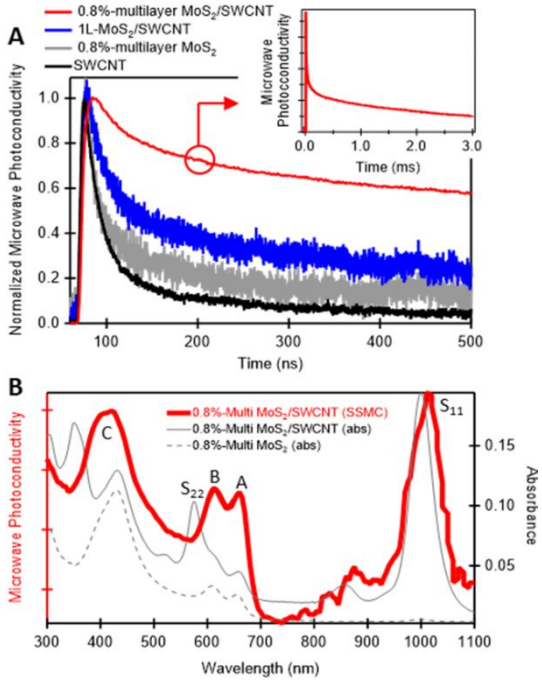

Figure 4. *(a) Normalized time-resolved microwave photoconductivity transients under 440nm excitation at 2 x 10^{12} absorbed photons cm^{-2} where the inset shows the transient on a longer time scale for the 0.8%-multilayer MoS_2/SWCNT heterojunction. (b) Comparison of steady-state microwave photoconductivity spectral response to absorption spectra of 0.8%-multilayer MoS_2/SWCNT and neat 0.8%-multilayer MoS_2. The peak labels indicate MoS_2 A, B, and C excitons along with SWCNT S_{11} and S_{22} transitions.*

Figure 4a shows significantly longer-lived TRMC signal on the 500 ns timescale for the 0.8%-multilayer MoS_2/SWCNT heterojunction compared to 1L-MoS_2/SWCNT, neat SWCNT, and neat 0.8%-multilayer MoS_2. Interestingly, we find that a photoconductivity signal in the 0.8%-multilayer MoS_2/SWCNT heterojunction persists even past several milliseconds (inset, Figure 4a), while there is no detectable signal for the other

samples in this time range. This result is consistent with recent results that show persistent photoconductivity lasting even up to several days, which was attributed to contributions from multilayer MoS_2 domains.[53] We note that longer lifetimes measured in TRMC compared to TA spectroscopy is not surprising, due to the higher sensitivity of the TRMC method and the selectivity toward mobile carriers which excludes contributions from quickly-decaying excitons. We also note that TA spectroscopy reveals an MoS_2 spectral signature in the 0.8%-multilayer MoS_2 samples that persists substantially longer than the other TA components (past the 100 μs time range, Figure S8), while the SWCNT-related trion TA signal decays around 10 μs (Figure 3a). These results suggest a mechanism in which the MoS_2 material plays a key role in sustaining long-lived mobile carriers when a small fraction of multilayer islands are present, potentially where carriers on MoS_2 continue to persist even after SWCNT-located carriers have decayed.

We further investigate the relative photoconductivity in the 0.8%-multilayer MoS_2/SWCNT heterojunction depending on whether the MoS_2 or SWCNT layer is initially photoexcited. Figure 4b compares the SSMC action spectrum to the absorption spectrum of 0.8%-multilayer MoS_2/SWCNT. The MoS_2 absorption features are disproportionately represented in the SSMC spectrum compared to their relative optical absorption in the heterojunction. Since the SSMC signal is proportional to $\varphi(\sum\mu)^2F_a$ (assuming a bimolecular recombination mechanism, where φ is the charge generation yield, μ is mobility, and F_a is the fraction of absorbed light),[48] the higher MoS_2 signal relative to the absorption implies that $\varphi(\sum\mu)^2$ is higher when MoS_2 is excited. The higher $\varphi(\sum\mu)^2$ at 440 nm excitation relative to 1000 nm excitation is consistent with our TA results (Table 2) that give higher φ_{CT} upon MoS_2 excitation compared to SWCNT excitation.

Spectral Signatures of Monolayer-Only versus Multilayer-Containing MoS_2

We next analyze the TA spectral signatures to gain further insight into the photophysical

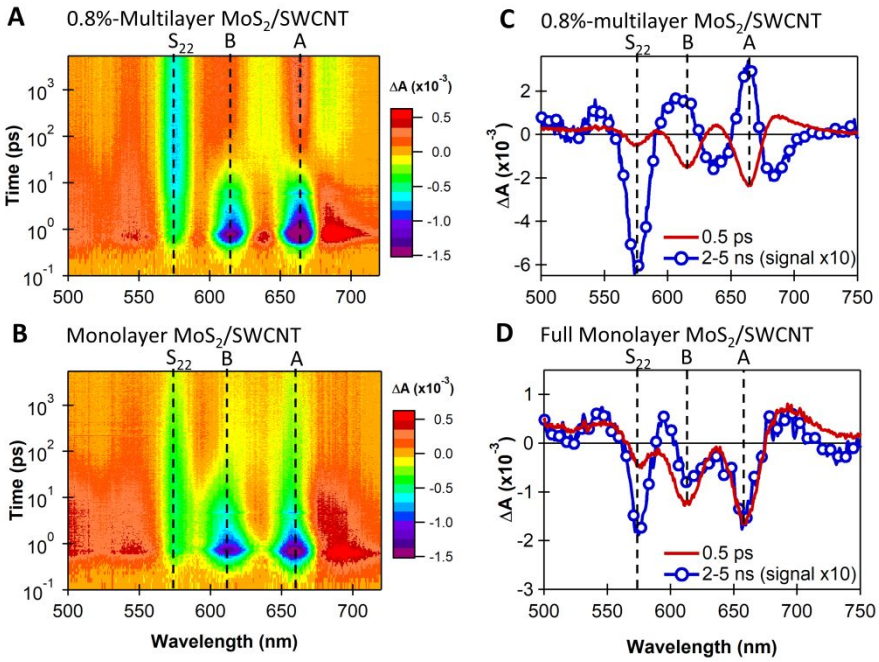

Figure 5. *Transient absorption (TA) spectra with 440 nm excitation at 1.2 x 10^{12} absorbed photons cm^{-2} from femtoseconds to 5 ns for (a) 0.8%-multilayer MoS_2/SWCNT and (b) large-area monolayer-only MoS_2/SWCNT. Comparison of TA spectra at 0.5 ps and 2-5 ns (spectra multiplied by 10) for (c) 0.8%-multilayer MoS_2/SWCNT, and (d) monolayer-only MoS_2/SWCNT.*

processes that underlie the exceptionally long-lived mobile charge carriers in the 0.8%-multilayer MoS_2/SWCNT heterojunctions.

Figures 5a and 5b show the evolution of the visible-range TA spectra over time for the 0.8%-multilayer and monolayer-only heterojunctions, respectively. At early times, both heterojunctions show similar bleach positions, which we assign to the MoS_2 A and B excitons (660 and 615 nm, respectively) along with the SWCNT S_{22} transition (575 nm). Interestingly, Figure 5a shows that the MoS_2 bleach signatures shift abruptly to longer wavelengths around 20 ps for the 0.8%-multilayer heterojunction, resulting in bleach positions at 685 and 640 nm. Figure S9 shows that this abrupt spectral shift also occurs in neat 0.8%-mutilayer MoS_2 samples. We do *not* observe this spectral shift in monolayer-only heterojunctions (Figure 5b) or monolayer-only neat MoS_2 (Figure S9). Figures 5c-d show a comparison of the spectra at 0.5 ps and averaged over 2-5 ns, highlighting the change in MoS_2 bleach positions that occurs only for the multilayer-containing samples.

Our results suggest that the abrupt shift of the MoS_2 bleach positions is related to the presence of multilayer sites, and it also appears to be correlated with the longer lifetimes in these multilayer-containing samples presented in Figures 3-4. In the Supporting Information (Section S5), we demonstrate the generality of this effect in a different set of predominately monolayer MoS_2/SWCNT samples that may contain multilayer islands. As we further describe below, we attribute the shifted spectral shape in the multilayer-containing samples primarily to electrons trapped in defect sites[11] while spectral overlap from non-trapped excitons and carriers can further affect the observed kinetics and relative intensities of the defect TA signatures. Our analysis below suggests that, while the shifted spectral shape is most likely a defect signature, it becomes enhanced and eventually saturated when populated by long-lived carriers that are formed by interfacial photoinduced charge transfer, leading to the exceptionally long lifetimes that we observe.

Probing Defect States at Multilayer Islands

Similar abrupt shifting of MoS_2 bleach positions (as shown in Figures 5a, 5c, and 5e) has been previously observed in few-layer MoS_2, and different studies have assigned this spectral change either to charge generation (even in the neat material)[54-56] or to mid-gap defect states that either serve as carrier traps or electron-hole recombination centers, depending on the relative capture rates and cross sections for electrons and holes.[6, 11-12, 57] We investigate these possibilities using the TA fluence dependence in our 0.8%-multilayer MoS_2 samples.

Figures 6a and 6b show neat 0.8%-multilayer MoS_2 at low fluence (5.5×10^{11} absorbed photons cm^{-2}) and high fluence (2.7×10^{12} absorbed photons cm^{-2}), respectively. The normalized spectral shapes are the same between the two fluences at early times (< 1 ps) and also at long delay times (2-5 ns). However, the abrupt spectral shift of MoS_2 bleach positions occurs an order of magnitude slower at high fluence (~100 ps) compared to low fluence (~10 ps). Figures 6c-d show corresponding 0.8%-multilayer MoS_2/SWCNT heterojunctions at the same low and high fluences. Again, we observe the abrupt spectral shift at both low and high fluence, but it occurs more slowly at higher fluence.

In addition to the slower spectral shift with higher fluence, the long-timescale (shifted) spectrum increases in intensity at the higher fluence (relative to low fluence) and with incorporation of the SWCNT layer (relative to neat 0.8%-multi MoS_2). Figures 6e-f highlight this trend using the kinetic traces at 665 nm (MoS_2 A-exciton bleach). The low-fluence kinetics in Figure 6e show a switch from bleaching to induced absorption around 10 ps, after which the induced absorption reaches higher

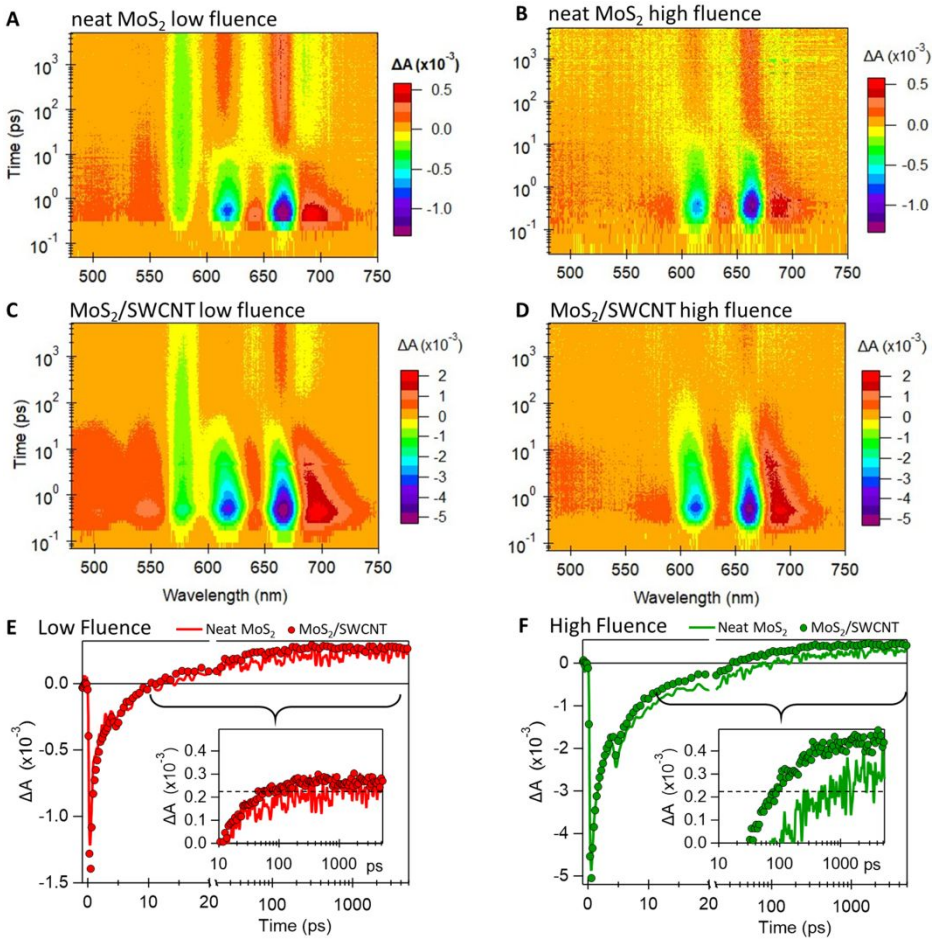

Figure 6. *Transient absorption spectra with 440 nm excitation from femtoseconds to 5 ns for (a) neat 0.8%-multilayer MoS_2 at low fluence (5.5 x 10^{11} absorbed photons cm^{-2}), (b) neat 0.8%-multilayer MoS_2 at high fluence (2.7 x 10^{12} absorbed photons cm^{-2}), (c) 0.8%-multilayer MoS_2/SWCNT at low fluence, (d) 0.8%-multilayer MoS_2/SWCNT at high fluence, along with kinetic traces probed at 665 nm at (e) low fluence and (d) high fluence with insets highlighting the kinetics between 10 ps to 5 ns. The dotted horizontal line in the insets is a guide to compare signal intensities to the average value of neat MoS_2 from 2-5 ns at low fluence.*

intensity in the heterojunction compared to the neat material. The horizontal dotted line in the inset is a guide to compare the induced absorption signal intensity to the average value of neat 0.8%-multi MoS_2 from 2-5 ns. Figure 5d shows that the bleach decays more slowly at high fluence, and the final induced absorption intensity reaches a higher value (see intensity comparison with horizontal dotted line in the inset).

If we assign the long-timescale (shifted) spectrum primarily to electrons localized in defects/traps, the fluence dependence shown in Figure 6e-f is consistent with trap filling.[6, 11-12, 57] That is, the defect-related induced absorption signature gains intensity when more traps are filled at higher excitation density. At low fluence, exciton quenching or charge capture at traps would lead to a relatively rapid bleach recovery. In contrast, the greater occupancy of traps at high fluence allows a larger fraction of excitons or charge carriers to avoid quenching at trap sites, leading to the slower bleach recovery.

The fluence dependence is *not* consistent with the induced absorption being a direct signature of free carriers that do not interact with trap states. For one, this shifted spectral signature shows a much slower 10-100 ps rise time compared to the ~0.5 ps rise time of carriers in

the SWCNT layer.[24] We also note that this signature is absent in 1L-only MoS_2/SWCNT heterojunctions that appear to generate charge relatively efficiently.[24] Furthermore, the timescale for charge generation *via* exciton dissociation should not become slower with increasing fluence. The charge-transfer time constant is most often fluence independent, although some processes such as exciton-exciton annihilation could lead to *faster* exciton quenching to generate charge.[4] We also note that this TA line-shape cannot be described by a typical Stark effect, as demonstrated in Figure S12 which shows that the spectrum cannot be reconstructed from the first or second derivatives of the ground-state absorption.

Despite this evidence that the induced absorption is not likely a direct signature of free charges, the heterojunction data in Figures 6c-d demonstrate that charge generation *via* intentional exciton dissociation across the heterojunction does *enhance* this long-timescale, shifted spectral signature. We propose that this is due to the charge carriers produced by interfacial exciton dissociation populating the defect states more efficiently than Coulomb-bound excitons can populate the defect states. That is, we propose that the defect is a carrier trap for one type of carrier (likely electrons) rather than an exciton recombination center that equally captures electrons and holes. In the case of the neat material, exciton recombination *via* radiative decay or other non-radiative decay pathways can compete with ionization and carrier trapping, decreasing the population of the defect states. In the heterojunction, many exciton recombination pathways are out-competed by charge transfer, which creates a greater density of long-lived electrons in MoS_2 that can become trapped without significant competition from other decay pathways. This results in a higher defect-related TA signal in the heterojunction samples compared to the neat 0.8%-multilayer MoS_2.

Our proposal that defect states play a significant role in the TA spectra implies that the defect-related signature should saturate at a pump fluence near the defect density. In Figure 7, we show the dependence on excitation fluence for the intensity of the defect-related induced absorption (blue traces) along with the initial bleach signal (red traces) for both neat 0.8%-multilayer MoS_2 and the heterojunction with SWCNTs. In both cases, we observe a maximum in the defect signal near 2.7 x 10^{12} cm^{-2} excitation density, which is consistent with the reported defect densities in the range of 10^{11} – 10^{13} cm^{-2} for MoS_2.[8, 11, 13, 18, 23, 57] The decrease in defect signal after 2.7 x 10^{12} cm^{-2} is due to increasing negative contribution from the longer-lasting MoS_2 bleach when the defect states become saturated. As noted above, we observe higher intensity of the defect-related signal at all fluences for the heterojunctions compared to the neat materials, which likely suggests charge carriers (likely electrons) populating the defect states rather than the defects acting as exciton recombination centers.

Despite the higher intensity of the defect-related induced absorption for the heterojunction, the early-timescale MoS_2 bleach signal (red circles, Figure 7) is similar between both the neat material and the heterojunction, suggesting similar density of initially-excited excitons in both cases. The magnitude of the early-time bleach signal increases sub-linearly with excitation fluence (N). Similar fluence dependence in monolayer[6] and bulk[58] MoS_2, other TMDCs like $MoSe_2$,[11, 59] and GaAs quantum wells[60] has been attributed to saturable absorption with $N/(N+N_s)$ fluence dependence, where N_s is the saturation density. Fitting our data to this model (dotted line in Figure 7) would suggest exciton saturation density of N_s = 5 to 6 x 10^{12} cm^{-2}, which is similar to the values proposed for $MoSe_2$ (~6 x 10^{12} cm^{-2})[11, 59] and MoS_2 (~1.6 x 10^{13} cm^{-2}).[6]

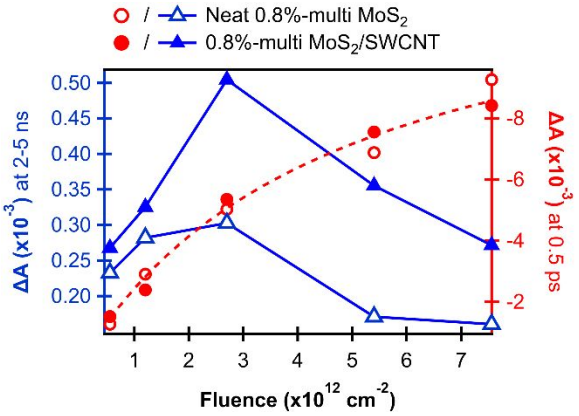

Figure 7. *Fluence (N) dependence of the defect-related induced absorption around 665 nm (blue triangles, left axis) averaged from 2-5 ns, along with the initial bleach intensity at 665 nm at 0.5 ps. Dotted line is a fit of the bleach intensity to a saturable absorption model $N/(N+N_S)$ with N_S = 5 x 10^{12} cm^{-2}.*

Conclusions

Here, we studied the effect of small changes in TMDC microstructure on charge generation in MoS_2/SWCNT heterojunctions. Our study was motivated by common observations of different photophysics for nominally similar TMDC-based heterojunctions, as well as the wide observations that small sample variations and presence of defect states can drastically alter photophysical processes and the resulting device performance in various optoelectronic or photochemical applications.

Our transient absorption spectroscopy studies showed that a small fraction of multilayer islands on predominately monolayer MoS_2 resulted in longer carrier lifetimes and higher charge transfer yields. We confirmed this result and specifically demonstrated the generation of *mobile* carriers using microwave photoconductivity, which showed a higher yield-mobility product when exciting at wavelengths absorbed by the 0.8%-multilayer MoS_2 *versus* those absorbed by the SWCNTs in the heterojunction. Surprisingly, we observed extremely long-live photoconductivity transients in the 0.8%-multilayer MoS_2/SWCNT heterojunctions, persisting past several milliseconds. To further understand this behavior in the 0.8%-multilayer MoS_2/SWCNT heterojunctions, we further investigated the TA spectral evolution and fluence dependence, which suggests a prominent role of charge trapping at defect states in the multilayer-containing material.

These results highlight the fascinating interplay between defects and microstructure in emerging TMDC materials with the resulting photophysics and efficiencies of mobile carrier generation. This understanding is an important step toward greater fundamental understanding of the significant roles defects play in electronic transport[18-19] and photocatalytic activity.[20-21]

Associated Content

Supporting Information

The following content is available online free of charge.

Experimental methods, atomic force microscopy (AFM) characterization, transient absorption fitting details and procedures, analysis of long-lived MoS_2 transient absorption signals, analysis of kinetics in heterojunctions between SWCNTs and CVD-grown MoS_2 flakes of varying size, comparison of transient absorption line-shapes with derivatives of the steady-state absorption.

Author Information

Corresponding Author

Jeffrey L. Blackburn jeffry.blackburn@nrel.gov

Author Contributions

The manuscript was written through contributions of all authors. D.B.S.-K. wrote the manuscript and performed experiments including photoluminescence and Raman mapping, microwave photoconductivity, transient absorption, and data fitting. H.Z. and Z.L. performed syntheses of MoS_2 materials and verification of material quality with Raman and photoluminescence. J.L.B. directed the work and helped to interpret results. All authors have given approval to the final version of the manuscript.

Acknowledgements

This work was authored in part by the Alliance for Sustainable Energy, LLC, the manager and operator of the National Renewable Energy Laboratory for the U.S. Department of Energy (DOE) under contract No. DE-AC36-08GO28308. Funding was provided by U.S. Department of Energy Office of Science Solar Photochemistry Program. The views expressed in this article do not necessarily represent the view of the DOE or the U.S. Government. The publisher, by accepting the article for publication, acknowledges that the U.S. Government retains a nonexclusive, paid-up, irrevocable, worldwide license to publish or reproduce the published form of this work, or allow others to do so, for U.S. Government purposes.

References

1. Sulas-Kern, D. B.; Miller, E. M.; Blackburn, J. L., Photoinduced Charge Transfer in Transition Metal Dichalcogenide Heterojunctions – Towards Next Generation Energy Technologies. *Energy Environ. Sci.* **2020,** *13*, 2684-2740.
2. Docherty, C. J.; Parkinson, P.; Joyce, H. J.; Chiu, M.-H.; Chen, C.-H.; Lee, M.-Y.; Li, L.-J.; Herz, L. M.; Johnston, M. B., Ultrafast Transient Terahertz Conductivity of Monolayer MoS2 and WSe2 Grown by Chemical Vapor Deposition. *ACS Nano* **2014,** *8* (11), 11147-11153.
3. Yuan, L.; Wang, T.; Zhu, T.; Zhou, M.; Huang, L., Exciton Dynamics, Transport, and Annihilation in Atomically Thin Two-Dimensional Semiconductors. *J. Phys. Chem. Lett.* **2017,** *8* (14), 3371-3379.
4. Sun, D.; Rao, Y.; Reider, G. A.; Chen, G.; You, Y.; Brézin, L.; Harutyunyan, A. R.; Heinz, T. F., Observation of Rapid Exciton–Exciton Annihilation in Monolayer Molybdenum Disulfide. *Nano Lett.* **2014,** *14* (10), 5625-5629.
5. Wang, H.; Zhang, C.; Rana, F., Surface Recombination Limited Lifetimes of Photoexcited Carriers in Few-Layer Transition Metal Dichalcogenide MoS2. *Nano Lett.* **2015,** *15* (12), 8204-8210.
6. Seo, M.; Yamaguchi, H.; Mohite, A. D.; Boubanga-Tombet, S.; Blancon, J.-C.; Najmaei, S.; Ajayan, P. M.; Lou, J.; Taylor, A. J.; Prasankumar, R. P., Ultrafast Optical Microscopy of Single Monolayer Molybdenum Disulfide Flakes. *Sci. Rep.* **2016,** *6* (1), 21601.
7. Shi, H.; Yan, R.; Bertolazzi, S.; Brivio, J.; Gao, B.; Kis, A.; Jena, D.; Xing, H. G.; Huang, L., Exciton Dynamics in Suspended Monolayer and Few-Layer MoS2 2D Crystals. *ACS Nano* **2013,** *7* (2), 1072-1080.
8. Cunningham, P. D.; McCreary, K. M.; Hanbicki, A. T.; Currie, M.; Jonker, B. T.; Hayden, L. M., Charge Trapping and Exciton Dynamics in Large-Area CVD Grown MoS2. *J. Phys. Chem. C* **2016,** *120* (10), 5819-5826.
9. Karmakar, M.; Bhattacharya, S.; Mukherjee, S.; Chowdhury, R. K.; Ray, S.; Datta, P. K. In *Effect of Size Confinement in C Exciton Dynamics of Few-Layered MoS2 Nano-Sheets*, SPIE Photonics Europe, SPIE: Strasbourg, France, 2018.
10. Chen, K.; Roy, A.; Rai, A.; Movva, H. C. P.; Meng, X.; He, F.; Banerjee, S. K.; Wang, Y., Accelerated carrier recombination by grain boundary/edge defects in MBE grown transition metal dichalcogenides. *APL Materials* **2018,** *6* (5), 056103.
11. Chen, K.; Ghosh, R.; Meng, X.; Roy, A.; Kim, J.-S.; He, F.; Mason, S. C.; Xu, X.; Lin, J.-F.; Akinwande, D.; Banerjee, S. K.; Wang, Y., Experimental evidence of exciton capture by mid-gap defects in CVD grown monolayer MoSe2. *NPJ 2D Mater. Appl.* **2017,** *1* (1), 15.
12. Chen, K.; Roy, A.; Rai, A.; Valsaraj, A.; Meng, X.; He, F.; Xu, X.; Register, L. F.; Banerjee, S.; Wang, Y., Carrier Trapping by Oxygen Impurities in Molybdenum Diselenide. *ACS Appl. Mater. Interfaces* **2018,** *10* (1), 1125-1131.
13. Wang, H.; Zhang, C.; Rana, F., Ultrafast Dynamics of Defect-Assisted Electron–Hole Recombination in Monolayer MoS2. *Nano Lett.* **2015,** *15* (1), 339-345.
14. H L, P.; Mondal, P.; Bid, A.; Basu, J. K., Electrical and Chemical Tuning of Exciton Lifetime in Monolayer MoS2 for Field-Effect Transistors. *ACS Appl. Nano Mater.* **2020,** *3* (1), 641-647.
15. McDonnell, S.; Addou, R.; Buie, C.; Wallace, R. M.; Hinkle, C. L., Defect-Dominated

Doping and Contact Resistance in MoS2. *ACS Nano* **2014,** *8* (3), 2880-2888.
16. Nie, Z.; Shi, Y.; Qin, S.; Wang, Y.; Jiang, H.; Zheng, Q.; Cui, Y.; Meng, Y.; Song, F.; Wang, X.; Turcu, I. C. E.; Wang, X.; Xu, Y.; Shi, Y.; Zhao, J.; Zhang, R.; Wang, F., Tailoring exciton dynamics of monolayer transition metal dichalcogenides by interfacial electron-phonon coupling. *Commun. Phys.* **2019,** *2* (1), 103.
17. Zhang, H.; Dunklin, J. R.; Reid, O. G.; Yun, S. J.; Nanayakkara, S. U.; Lee, Y. H.; Blackburn, J. L.; Miller, E. M., Disentangling oxygen and water vapor effects on optoelectronic properties of monolayer tungsten disulfide. *Nanoscale* **2020,** *12* (15), 8344-8354.
18. Qiu, H.; Xu, T.; Wang, Z.; Ren, W.; Nan, H.; Ni, Z.; Chen, Q.; Yuan, S.; Miao, F.; Song, F.; Long, G.; Shi, Y.; Sun, L.; Wang, J.; Wang, X., Hopping transport through defect-induced localized states in molybdenum disulphide. *Nat. Commun.* **2013,** *4* (1), 2642.
19. Yang, M.; Kim, T.-Y.; Lee, T.; Hong, S., Nanoscale enhancement of photoconductivity by localized charge traps in the grain structures of monolayer MoS2. *Sci. Rep.* **2018,** *8* (1), 15822.
20. Li, G.; Zhang, D.; Qiao, Q.; Yu, Y.; Peterson, D.; Zafar, A.; Kumar, R.; Curtarolo, S.; Hunte, F.; Shannon, S.; Zhu, Y.; Yang, W.; Cao, L., All The Catalytic Active Sites of MoS2 for Hydrogen Evolution. *J. Am. Chem. Soc.* **2016,** *138* (51), 16632-16638.
21. Li, H.; Du, M.; Mleczko, M. J.; Koh, A. L.; Nishi, Y.; Pop, E.; Bard, A. J.; Zheng, X., Kinetic Study of Hydrogen Evolution Reaction over Strained MoS2 with Sulfur Vacancies Using Scanning Electrochemical Microscopy. *J. Am. Chem. Soc.* **2016,** *138* (15), 5123-5129.
22. Atallah, T. L.; Wang, J.; Bosch, M.; Seo, D.; Burke, R. A.; Moneer, O.; Zhu, J.; Theibault, M.; Brus, L. E.; Hone, J.; Zhu, X. Y., Electrostatic Screening of Charged Defects in Monolayer MoS2. *J. Phys. Chem. Lett.* **2017,** *8* (10), 2148-2152.
23. Hong, J.; Hu, Z.; Probert, M.; Li, K.; Lv, D.; Yang, X.; Gu, L.; Mao, N.; Feng, Q.; Xie, L.; Zhang, J.; Wu, D.; Zhang, Z.; Jin, C.; Ji, W.; Zhang, X.; Yuan, J.; Zhang, Z., Exploring atomic defects in molybdenum disulphide monolayers. *Nat. Commun.* **2015,** *6* (1), 6293.
24. Sulas-Kern, D. B.; Zhang, H.; Li, Z.; Blackburn, J. L., Microsecond Charge Separation at Heterojunctions Between Transition Metal Dichalcogenide Monolayers and Single-Walled Carbon Nanotubes. *Mater. Horiz.* **2019**.
25. Zhu, T.; Yuan, L.; Zhao, Y.; Zhou, M.; Wan, Y.; Mei, J.; Huang, L., Highly mobile charge-transfer excitons in two-dimensional WS2/tetracene heterostructures. *Sci. Adv.* **2018,** *4* (1), eaao3104.
26. Bettis Homan, S.; Sangwan, V. K.; Balla, I.; Bergeron, H.; Weiss, E. A.; Hersam, M. C., Ultrafast Exciton Dissociation and Long-Lived Charge Separation in a Photovoltaic Pentacene–MoS2 van der Waals Heterojunction. *Nano Lett.* **2017,** *17* (1), 164-169.
27. Kafle, T. R.; Kattel, B.; Yao, P.; Zereshki, P.; Zhao, H.; Chan, W.-L., Effect of the Interfacial Energy Landscape on Photoinduced Charge Generation at the ZnPc/MoS2 Interface. *J. Am. Chem. Soc.* **2019,** *141* (28), 11328-11336.
28. Padgaonkar, S.; Amsterdam, S. H.; Bergeron, H.; Su, K.; Marks, T. J.; Hersam, M. C.; Weiss, E. A., Molecular-Orientation-Dependent Interfacial Charge Transfer in Phthalocyanine/MoS2 Mixed-Dimensional Heterojunctions. *J. Phys. Chem. C* **2019**.
29. Kim, J.-K.; Cho, K.; Kim, T.-Y.; Pak, J.; Jang, J.; Song, Y.; Kim, Y.; Choi, B. Y.; Chung, S.; Hong, W.-K.; Lee, T., Trap-mediated electronic transport properties of gate-tunable pentacene/MoS2 p-n heterojunction diodes. *Sci. Rep.* **2016,** *6*, 36775.
30. Petoukhoff, C. E.; Kosar, S.; Goto, M.; Bozkurt, I.; Chhowalla, M.; Dani, K. M., Charge transfer dynamics in conjugated polymer/MoS2 organic/2D heterojunctions. *Mol. Syst. Des. Eng.* **2019,** *4* (4), 929-938.
31. Zhong, C.; Sangwan, V. K.; Wang, C.; Bergeron, H.; Hersam, M. C.; Weiss, E. A., Mechanisms of Ultrafast Charge Separation in a PTB7/Monolayer MoS2 van der Waals Heterojunction. *J. Phys. Chem. Lett.* **2018,** *9* (10), 2484-2491.

32. Mak, K. F.; Lee, C.; Hone, J.; Shan, J.; Heinz, T. F., Atomically Thin MoS2 A New Direct-Gap Semiconductor. *Phys. Rev. Lett.* **2010,** *105* (13), 136805.
33. Tosun, M.; Fu, D.; Desai, S. B.; Ko, C.; Seuk Kang, J.; Lien, D.-H.; Najmzadeh, M.; Tongay, S.; Wu, J.; Javey, A., MoS2 Heterojunctions by Thickness Modulation. *Sci. Rep.* **2015,** *5*, 10990.
34. Xia, C.; Xiong, W.; Du, J.; Wang, T.; Peng, Y.; Wei, Z.; Li, J.; Jia, Y., Type-I Transition Metal Dichalcogenides Lateral Homojunctions: Layer Thickness and External Electric Field Effects. *Small* **2018,** *14* (21), 1800365.
35. Howell, S. L.; Jariwala, D.; Wu, C.-C.; Chen, K.-S.; Sangwan, V. K.; Kang, J.; Marks, T. J.; Hersam, M. C.; Lauhon, L. J., Investigation of Band-Offsets at Monolayer–Multilayer MoS2 Junctions by Scanning Photocurrent Microscopy. *Nano Lett.* **2015,** *15* (4), 2278-2284.
36. He, Y.; Sobhani, A.; Lei, S.; Zhang, Z.; Gong, Y.; Jin, Z.; Zhou, W.; Yang, Y.; Zhang, Y.; Wang, X.; Yakobson, B.; Vajtai, R.; Halas, N. J.; Li, B.; Xie, E.; Ajayan, P., Layer Engineering of 2D Semiconductor Junctions. *Adv. Mater.* **2016,** *28* (25), 5126-5132.
37. Mouri, S.; Miyauchi, Y.; Matsuda, K., Tunable Photoluminescence of Monolayer MoS2 via Chemical Doping. *Nano Lett.* **2013,** *13* (12), 5944-5948.
38. Brivio, J.; Alexander, D. T. L.; Kis, A., Ripples and Layers in Ultrathin MoS2 Membranes. *Nano Lett.* **2011,** *11* (12), 5148-5153.
39. Wang, J.; Namburu, R. R.; Dubey, M.; Dongare, A. M., Origins of Ripples in CVD-Grown Few-layered MoS2 Structures under Applied Strain at Atomic Scales. *Sci. Rep.* **2017,** *7* (1), 40862.
40. Su, L.; Yu, Y.; Cao, L.; Zhang, Y., In Situ Monitoring of the Thermal-Annealing Effect in a Monolayer of MoS2. *Physical Review Applied* **2017,** *7* (3), 034009.
41. Jia, Y.; Stanev, T. K.; Lenferink, E. J.; Stern, N. P., Enhanced conductivity along lateral homojunction interfaces of atomically thin semiconductors. *2D Mater.* **2017,** *4* (2), 021012.
42. Padilha, J. E.; Peelaers, H.; Janotti, A.; Van de Walle, C. G., Nature and evolution of the band-edge states in MoS2: From monolayer to bulk. *Phys. Rev. B* **2014,** *90* (20), 205420.
43. Park, S.; Mutz, N.; Schultz, T.; Blumstengel, S.; Han, A.; Aljarb, A.; Li, L.-J.; List-Kratochvil, E. J. W.; Amsalem, P.; Koch, N., Direct determination of monolayer MoS2 and WSe2 exciton binding energies on insulating and metallic substrates. *2D Mater.* **2018,** *5* (2), 025003.
44. Park, S.; Schultz, T.; Xu, X.; Wegner, B.; Aljarb, A.; Han, A.; Li, L.-J.; Tung, V. C.; Amsalem, P.; Koch, N., Demonstration of the key substrate-dependent charge transfer mechanisms between monolayer MoS2 and molecular dopants. *Commun. Phys.* **2019,** *2* (1), 109.
45. Guo, Y.; Robertson, J., Band engineering in transition metal dichalcogenides: Stacked versus lateral heterostructures. *Appl. Phys. Lett.* **2016,** *108* (23), 233104.
46. Schlaf, R.; Lang, O.; Pettenkofer, C.; Jaegermann, W., Band lineup of layered semiconductor heterointerfaces prepared by van der Waals epitaxy: Charge transfer correction term for the electron affinity rule. *J. Appl. Phys.* **1999,** *85* (5), 2732-2753.
47. Kang, H. S.; Sisto, T. J.; Peurifoy, S.; Arias, D. H.; Zhang, B.; Nuckolls, C.; Blackburn, J. L., Long-Lived Charge Separation at Heterojunctions between Semiconducting Single-Walled Carbon Nanotubes and Perylene Diimide Electron Acceptors. *J. Phys. Chem. C* **2018,** *122* (25), 14150-14161.
48. Reid, O. G.; Moore, D. T.; Li, Z.; Zhao, D.; Yan, Y.; Zhu, K.; Rumbles, G., Quantitative analysis of time-resolved microwave conductivity data. *J. Phys. D: Appl. Phys.* **2017,** *50* (49), 493002.
49. Kunst, M.; Beck, G., The study of charge carrier kinetics in semiconductors by microwave conductivity measurements. *J. Appl. Phys.* **1986,** *60* (10), 3558-3566.
50. Ahrenkiel, R. K.; Johnston, S. W., An advanced technique for measuring minority-carrier parameters and defect properties of

semiconductors. *Materials Science and Engineering: B* **2003,** *102* (1), 161-172.
51. Schüler, N.; Mittelstrass, D.; Dornich, K.; Niklas, J. R.; Neuhaus, H. In *Next generation inline minority carrier lifetime metrology on multicrystalline silicon bricks for PV*, 35th IEEE Photovoltaic Specialists Conference, 2010; pp 000852-000857.
52. Johnston, S.; Yan, F.; Zaunbrecher, K.; Al-Jassim, M.; Sidelkheir, O.; Ounadjela, K. In *Quality characterization of silicon bricks using photoluminescence imaging and photoconductive decay*, 2012 38th IEEE Photovoltaic Specialists Conference, 3-8 June 2012; 2012; pp 000406-000410.
53. Berweger, S.; Zhang, H.; Sahoo, P. K.; Kupp, B. M.; Blackburn, J. L.; Miller, E. M.; Wallis, T. M.; Voronine, D. V.; Kabos, P.; Nanayakkara, S. U., Spatially Resolved Persistent Photoconductivity in MoS2–WS2 Lateral Heterostructures. *ACS Nano* **2020,** *14* (10), 14080-14090.
54. Borzda, T.; Gadermaier, C.; Vujicic, N.; Topolovsek, P.; Borovsak, M.; Mertelj, T.; Viola, D.; Manzoni, C.; Pogna, E. A. A.; Brida, D.; Antognazza, M. R.; Scotognella, F.; Lanzani, G.; Cerullo, G.; Mihailovic, D., Charge Photogeneration in Few-Layer MoS2. *Adv. Funct. Mater.* **2015,** *25* (22), 3351-3358.
55. Yu, X.; Rahmanudin, A.; Jeanbourquin, X. A.; Tsokkou, D.; Guijarro, N.; Banerji, N.; Sivula, K., Hybrid Heterojunctions of Solution-Processed Semiconducting 2D Transition Metal Dichalcogenides. *ACS Energy Lett.* **2017,** *2* (2), 524-531.
56. Tsokkou, D.; Yu, X.; Sivula, K.; Banerji, N., The Role of Excitons and Free Charges in the Excited-State Dynamics of Solution-Processed Few-Layer MoS2 Nanoflakes. *J. Phys. Chem. C* **2016,** *120* (40), 23286-23292.
57. Ke, D.; Sui, L.-z.; Liu, D.-l.; Cui, J.-q.; Zhang, Y.-f.; Li, Q.-y.; Li, S.-y.; Jiang, Y.-f.; Chen, A.-m.; Song, J.-l.; Jin, M.-x., Ultrafast dynamics of defect-assisted carrier capture in MoS2 nanodots investigated by transient absorption spectroscopy. *Chin. J. Chem. Phys.* **2018,** *31* (3), 277-283.
58. Kumar, N.; He, J.; He, D.; Wang, Y.; Zhao, H., Charge carrier dynamics in bulk MoS2 crystal studied by transient absorption microscopy. *J. Appl. Phys.* **2013,** *113* (13), 133702.
59. Kumar, N.; Cui, Q.; Ceballos, F.; He, D.; Wang, Y.; Zhao, H., Exciton-exciton annihilation in MoSe2 monolayers. *Phys. Rev. B* **2014,** *89* (12), 125427.
60. Hunsche, S.; Leo, K.; Kurz, H.; Köhler, K., Exciton absorption saturation by phase-space filling: Influence of carrier temperature and density. *Phys. Rev. B* **1994,** *49* (23), 16565-16568.